

# Synthesis and characterization of novel hybrid nanomaterials based on $\beta$ -cyclodextrine grafted halloysite nanotubes for delivery of doxorubicin to MCF-7 cell line

Vahid Shafiei-Irannejad<sup>a</sup>, Vahid Rahimkhoei<sup>b</sup>, Morteza Molaparast<sup>a</sup>, Ali Akbari<sup>b,\*</sup>

<sup>a</sup> Cellular and Molecular Research Center, Cellular and Molecular Medicine Institute, Urmia University of Medical Sciences, Urmia, Iran

<sup>b</sup> Solid Tumor Research Center, Cellular and Molecular Medicine Institute, Urmia University of Medical Sciences, Urmia, Iran

## ARTICLE INFO

### Article history:

Received 25 December 2021

Revised 3 April 2022

Accepted 4 April 2022

Available online 5 April 2022

### Keyword:

Halloysite nanotubes

Surface modification

Anticancer drug

Blood compatibility and drug delivery system

## ABSTRACT

In the present study, the surface of halloysite nanotubes (Hal) grafted with a reactive  $\beta$ -cyclodextrin based monomer carrying vinyl carboxylic acid functional groups (MAH- $\beta$ -CD) was designed and prepared through free radical copolymerization (Hal-V/MAH- $\beta$ -CD) for anticancer drug delivery. Doxorubicin (DOX) was loaded effectively to the Hal-V/MAH- $\beta$ -CD nanocarrier via physical adsorption with high loading efficiency. Drug release investigations demonstrated that DOX@Hal-V/MAH- $\beta$ -CD nanocarrier has a high drug release at cancerous condition (pH 5.4). From MTT assay, it was found that DOX@Hal-V/MAH- $\beta$ -CD exerted great anticancer effect against MCF-7 breast cancer cells. The hemolysis experiments exhibited that nanocarrier has no remarkable hemolytic effect on human red blood cells (HRBCs), indicating the blood compatibility of the nanocarrier. Taken together, the newly prepared Hal-V/MAH- $\beta$ -CD nanocarrier can be considered as a promising tool for DOX delivery to the MCF-7 breast cancer cells.

© 2022 Elsevier B.V. All rights reserved.

## 1. Introduction

Nowadays, breast cancer (BC) is known as one of the most life threatening women's cancer in the world and currently about 12% of cancers in women is related to the BC [1,2]. Beside surgery, radiation therapy and hormonal therapy, chemotherapy still plays a key role in BC treatment. In this regard, some chemotherapeutic agents such as paclitaxel (PTX), 5-fluorouracil (5-FU) and doxorubicin (DOX) are frequently used in clinics. Among them, doxorubicin (DOX) is an important anthracycline antibiotic with excellent therapeutic properties for treatment of various cancers including breast cancer [3]. Although, DOX showed a high chemotherapeutic effect towards different cancer cells, its clinical application has been limited by various parameters including nonspecific distribution and short biological half-period which leads to remarkable side effects such as vomiting, diarrhea, nausea and congestive heart failure [4–6]. In the past few decades, nanotechnology had a great impact on development of novel safe biocompatible drug delivery systems with low toxicity for cancer therapy. Thus, by rapid development in nanotechnology, a variety of nanocarriers such as organic and inorganic nanocarriers have been developed and applied for DOX delivery to specific types of can-

cer cells [7–9]. Halloysite (Hal) nanotubes as economically available natural two-layered aluminosilicate deposits with the chemical formula of  $\text{Al}_2\text{Si}_2\text{O}_5(\text{OH})_4 \cdot n\text{H}_2\text{O}$  (where n is 4 or 2) have attracted remarkable attention in drug delivery and cancer therapy [10]. Hal nanotubes have the following characteristics: (1) hollow tubular structure with length of 200–1000 nm and diameter of 50–70 nm; (2) high thermal and mechanical stability; (3) high adsorption capacity; (4) ease of dispersion within polymers; (5) facile surface modification ability; (6) low toxicity and biocompatibility [10,11]. However, uncontrolled drug release profile limited its applications in drug delivery [12]. Therefore, Hal nanotubes have been usually combined with other biomolecules and biopolymers such as L-dopa, chitosan, PVA, PLA, PLGA and PEG to generate new inorganic/polymer hybrid materials with controlled drug release behavior [10]. For example, chitosan oligosaccharide-grafted Hal (Hal-g-COS) hybrid materials were synthesized and used as DOX carrier for efficient breast cancer therapy both in vitro and in vivo [13]. The same research group could successfully conjugate PEG and FA on the surface of Hal nanotubes for effectively delivering DOX to breast cancer [14]. In other interesting reports, Hal nanotubes were modified with polyamidoamine (PAMAM) and polyethyleneimine (PEI) as promising nanovehicles for siRNA and pDNA delivery, respectively [15,16]. Very recently, we have successfully functionalized Hal surface with water soluble polyhedral oligomeric silsesquioxane nanoparticles for paclitaxel delivery into

\* Corresponding author.

E-mail address: [Akbari.a@umsu.ac.ir](mailto:Akbari.a@umsu.ac.ir) (A. Akbari).

the cancer cells [17]. In recent years,  $\beta$ -cyclodextrin ( $\beta$ -CD) and its derivatives have received great interest due to the properties possessed by them, for instance, unique conical scaffold, biocompatibility, nontoxic nature and cost-effectiveness [18]. The remarkable feature of  $\beta$ -CD that allows the development of new drug carriers in controlled release systems is not only its capability for increasing the solubilization and stabilization of hydrophobic drugs, but also decreasing the uncontrolled side effects related to the corresponding drugs [19,20]. According to these features,  $\beta$ -CD can be considered as a promising candidate in the preparation of hybrid materials for the storage and delivery of anticancer drugs. However, through literature review, we noticed that there are few studies on the surface functionalization of Hal nanotubes with  $\beta$ -CD and its biomedical application. In one report, carboxylated  $\beta$ -CD was covalently coated on the surface of magnetic aminolated Hal nanotubes using EDC chemistry and used to capture and isolate the cancer cells from normal cells [21]. In continuation of our interest in the preparation of hybrid materials and their application in various fields [22–38], herein, we designed and fabricated a new Hal based hybrid material (Hal-V/MAH- $\beta$ -CD) as an efficient nanocarrier for DOX delivery into the cancer cells for the first time. Firstly, Hal nanotubes and  $\beta$ -CD were functionalized with 3-(trimethoxysilyl)propyl methacrylate and maleic anhydride to obtain Hal-V and MAH- $\beta$ -CD as active polymerizable monomers, respectively. Secondly, Hal-V was modified with MAH- $\beta$ -CD by a simple free radical copolymerization to prepare Hal-V/MAH- $\beta$ -CD nanocarrier. Finally, DOX as a widely used anticancer drug was loaded onto Hal-V/MAH- $\beta$ -CD via adsorption. The successful preparation of Hal-V/MAH- $\beta$ -CD was approved using various characterization methods. In addition, DOX@Hal-V/MAH- $\beta$ -CD was subjected to biological studies including hemolysis assay, cytotoxicity evaluations and cellular uptake.

## 2. Materials and methods

### 2.1. Materials

Halloysite nanotubes (Hal) and  $\beta$ -cyclodextrin ( $\beta$ -CD), 3-(4, 5-dimethylthiazole-2-yl)-2, 5-di-phenyl tetrazolium bromide (MTT), toluene, and doxorubicin were obtained from Sigma-Aldrich (Germany). Maleic anhydride (MAH), Redox Initiator ammonium persulfate (APS), 3-(trimethoxysilyl)propyl methacrylate, and *N,N*-methylenebis (acrylamide) (MBA) were purchased from Merck (Germany). All other chemicals were analytical grade and used as received.

### 2.2. Functionalization of Hal with 3-(trimethoxysilyl)propyl methacrylate: preparation of Hal-V

Initially, Hal surface was functionalized with 3-(trimethoxysilyl)propyl methacrylate. Generally, 3-(trimethoxysilyl)propyl methacrylate (8 mL) was added drop wise into a 250 mL beaker equipped with a magnetic stirrer containing a suspension of Hal (4.8 g) in dry toluene (120 mL), and allowed to stir vigorously for 15 min. Subsequently, the reaction mixture was refluxed at 110 °C overnight. After completion of the reaction, the product (Hal-V) was filtered off, washed three times with dried toluene and dried under vacuum at 100 °C for 24 h.

### 2.3. Preparation of $\beta$ -CD based reactive monomer (MAH- $\beta$ -CD)

At first,  $\beta$ -CD (2.84 g, 0.0025 mol) was dissolved in DMF (20 mL), then MAH (2.45 g, 0.025 mol) was added into the reaction mixture under inert atmosphere and stirred to obtain transparent solution. This solution was stirred vigorously at 100 °C for 10 h. After that the reaction mixture was allowed to cooling at room

temperature, followed by adding 25 mL of chloroform. Obtained white precipitate (named MAH- $\beta$ -CD) was washed several times using 100 mL acetone, dried under vacuum at 80 °C overnight.

### 2.4. Decoration of Hal surface with MAH- $\beta$ -CD: synthesis of Hal-V/MAH- $\beta$ -CD

To synthesize the copolymerized nanocarrier, Hal-V (1.2 g) was dispersed in distilled water under ultrasonic irradiation of power 100 W for 15 min. To the resulting suspension, MAH- $\beta$ -CD (1.2 g) and MBA (0.1 g) were added and the reaction temperature was increased to 70 °C. Following this, APS (0.04 g) as polymerization initiator was added to allow the polymerization proceed. After 24 h, the formed nanocarrier was centrifuged and washed with distilled water repeatedly to remove unreacted monomers. The obtained product was dried in a vacuum oven at 100 °C to reach constant weight and assigned as Hal-V/MAH- $\beta$ -CD.

### 2.5. In-vitro drug loading and drug release investigations

DOX loading on the Hal-V/MAH- $\beta$ -CD was conducted according to the following procedure: 100 mg of Hal-V/MAH- $\beta$ -CD was added in 10 mL DOX solution (10 mg DOX in PBS, pH = 7.4) and ultrasonically dispersed in the iced bath. The mixture was allowed to stir at room temperature for 24 h under dark condition. DOX@Hal-V/MAH- $\beta$ -CD was separated by centrifugation and washed several times with PBS to eliminate unloaded DOX. At the end, DOX-nanocarrier was freeze-dried and kept for the next *in-vitro* studies. To measure the amount of unbounded DOX, the supernatant of above solution was collected and analyzed for the concentration of DOX left using a UV-Vis spectrophotometer at 480 nm according to the calibration curve (Fig 1S). The drug loading efficiency (DLE) and drug encapsulation efficiency (DEE) were calculated using the following equations [39]:

$$DLE (\%) = \frac{\text{Weight of drug in nanocarrier (mg)}}{\text{Weight of nanocarrier (mg)}} \times 100$$

$$DEE (\%) = \frac{\text{Weight of initially added drug} - \text{weight of free drug in supernatant}}{\text{Weight of initially added drug}} \times 100$$

To study the in-vitro release profile of DOX from Hal-V/MAH- $\beta$ -CD nanocarrier, 10 mg of DOX-loaded nanocarrier was suspended in a 2 mL of phosphate buffered saline (PBS) at two different pH values (5.4 and 7.4) as the release medium. At certain time intervals, 2 mL of release medium was replaced with 2 mL of fresh medium. Finally, the concentration of released DOX was measured using a UV-Vis spectrophotometer at 480 nm. All release experiments were carried out in triplicate, and the average data was reported.

$$DOX \text{ Release } (\%) = \frac{\text{amount of DOX released in medium}}{\text{amount of DOX in nanocarrier}} \times 100$$

### 2.6. Cell culture and cytotoxicity studies

Human breast cancer cell lines (MCF-7) were grown according to the protocol as previously reported in the literature [40]. Briefly, MCF-7 cells were cultured in Gibco® RPMI-1640 containing 10% fetal bovine serum (FBS) and 1% benzylpenicillin/streptomycin and incubated at 37 °C for 24 h under a humidified atmosphere with 5% CO<sub>2</sub>. MTT assay was used to assess the in-vitro cytotoxic effects of free drug and drug-loaded nanocarrier on MCF-7 cells. MCF-7 cells were seeded in a flat-bottomed 96-well plates at the density of 5 × 10<sup>3</sup> per well and incubated overnight (37 °C, 5% CO<sub>2</sub>). Then, MCF-7 cells were treated with pristine DOX and DOX@Hal-V/MAH- $\beta$ -CD nanocarriers at various concentrations (62.5, 125,

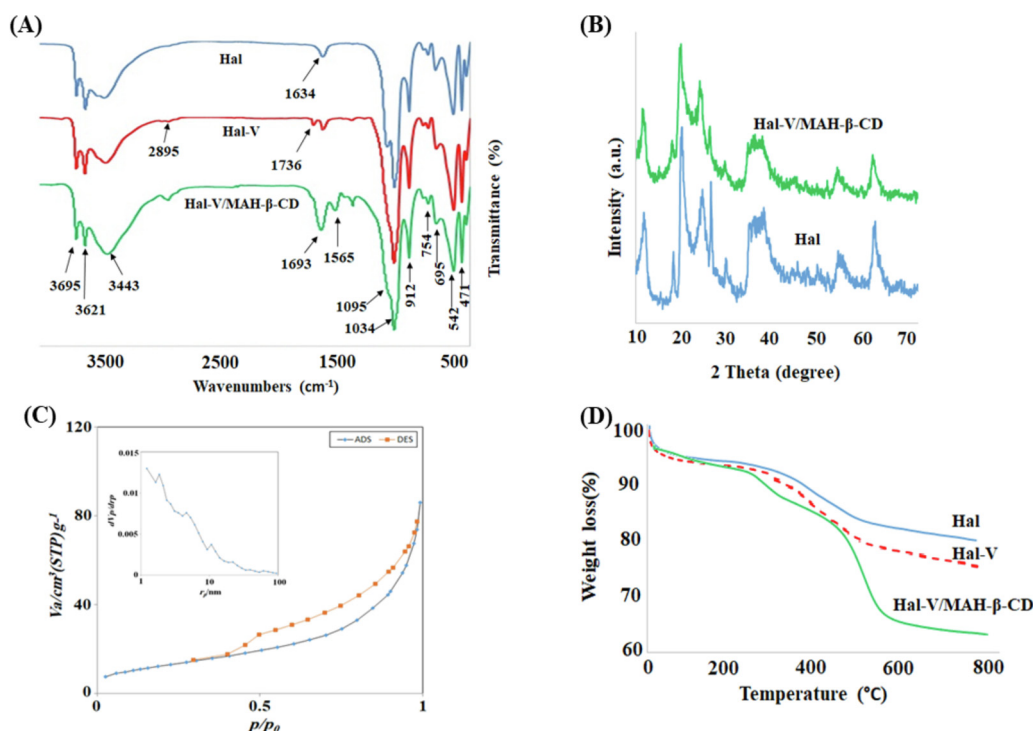


**Fig. 1.** FTIR spectra of the Hal, Hal-V, Hal-V/MAH-β-CD (A), XRD pattern of Hal, Hal-V/MAH-β-CD (B), N<sub>2</sub> adsorption-desorption isotherm of Hal-V/MAH-β-CD (C), Thermal gravimetric analysis (TGA) curves of Hal, Hal-V, Hal-V/MAH-β-CD (D).

250, 500, 1000 and 2000 μM) and incubated at temperature 37 °C. After 24 h, the media were replaced with 50 μL MTT solution (2mgmL<sup>-1</sup>) and 150 μL of fresh culture media, and incubated at 37 °C for another 4 h. After removing of the medium in each well, appropriate DMSO was added to each well to solve the formazan precipitates. Finally, ELISA plate reader (Awareness Technology, Palm City, FL, USA) was employed to determine the optical density (OD) at 570 nm. Following equation was used to calculate the percentage viability of cell.

$$\text{Cell viability (\%)} = \frac{\text{OD (treated)}}{\text{OD (control)}} \times 100$$

## 2.7. Statistical analysis

For cell culture experiments, statistical analysis was performed using the IBM Statistical Package for the Social Sciences Statistical software (SPSS, version 16.0). All experiments were done in triplicate. Experimental data were presented as mean ± standard deviation. One-way Analysis of Variance (ANOVA) and Tukey's test for posthoc analysis were used to calculate statistical differences between multiple groups. *P* values < 0.01 and 0.05 were considered statistically significant.

## 2.8. In-vitro blood compatibility: hemolysis assay

Human blood was kindly donated by the Iranian Blood Transfusion Institute (IBTI) and then centrifuged at 2500 rpm for 10 min to obtain human red blood cells (HRBCs), followed by washing several times with PBS to become the supernatant of the sample clear. Ten times diluted HRBCs (0.5 mL) by PBS were mixed with 0.5 mL of nanocarrier suspension with different concentrations in PBS (the final nanocarrier concentration: 10, 25, 50, 100, 200, 400, 800, 1600 μgmL<sup>-1</sup>) in test tubes. Moreover, the mixture of 0.5 mL of HRBCs suspension with 0.5 mL of deionized water and PBS were assigned as the positive (100% hemolysis rate) and negative controls (0% hemolysis rate), respectively. All prepared samples were

stirred gently at 37 °C for 4 h. After separation using centrifuge, all separated supernatants were taken up and subjected to ELISA-reader to measure the OD of released hemoglobin at 540 nm. The hemolysis rate (%) was calculated based on the following equation:

$$\text{Hemolysis rate (\%)} = \frac{\text{OD (sample)} - \text{OD (-)}}{\text{OD (+)} - \text{OD (-)}} \times 100$$

## 2.9. Cellular uptake study: using fluorescent microscopy imaging

Fluorescent microscopy imaging was used to assess the internalization of the DOX@Hal-V/MAH-β-CD nanocarrier into the cells. Briefly, seeded and incubated MCF-7 cells (6 × 10<sup>4</sup>) in a 6-well plate containing coverslips were treated with DOX-loaded nanocarrier at a concentration of IC<sub>50</sub> for 0.5, 1, 2, and 3 h. To observe nanocarrier uptake by cells, the coverslips were put and fixed onto the glass microscope slides, followed by recording images using a fluorescence microscope (Olympus microscope Bh2-RFCA, Japan).

## 2.10. Instruments

### 2.10.1. Fourier transform infrared spectroscopy (FT-IR)

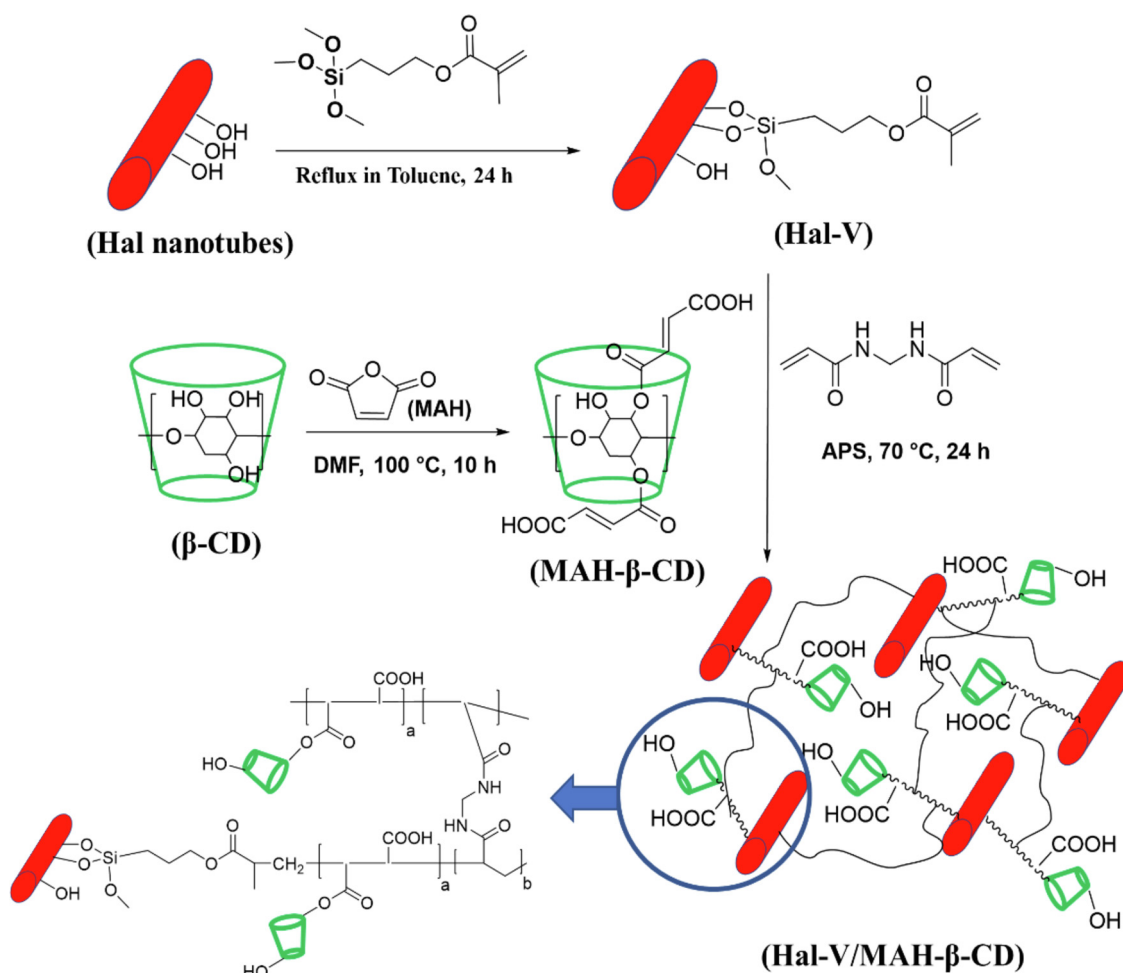
Fourier transform infrared (FT-IR) spectra were recorded on a Win-Bomem spectrometer, version 3.04 Galactic Industries Corporation over the range of 400–4000 cm<sup>-1</sup>.

### 2.10.2. Hydrogen nuclear resonance (<sup>1</sup>H NMR)

The <sup>1</sup>H NMR spectrum of samples were recorded on a Bruker FT-NMR 500 MHz spectrometer in D<sub>2</sub>O solvent.

### 2.10.3. Wide-angle X-ray diffraction (XRD)

The XRD diffraction patterns of samples were collected with a Bruker D8 Advance diffractometer using a Cu Kα radiation source (λ = 0.154059 nm) at 30 keV in the scan range (2θ) from 4 to 70°



**Scheme 1.** Schematic illustration of possible procedures for the synthesis of Hal-V/MAH-β-CD.

#### 2.10.4. $N_2$ adsorption-desorption analysis

$N_2$  adsorption-desorption isotherm was recorded using BEL-SORP Mini II apparatus

#### 2.10.5. Thermogravimetric analysis (TGA)

Thermogravimetric (TGA) analyses were carried out using a Linseis L81A1750 (Germany) at a heating rate of 10 °C/min under high purity nitrogen atmosphere from 50 to 800 °C.

#### 2.10.6. Scanning electron microscopy (SEM)

The morphology of the samples were examined using VWGA3 TESCAN (20.0 KV) microscope field emission scanning electron microscope (FE-SEM) at an accelerating voltage of 20 keV with an energy-dispersive X-ray (EDX) microanalyzer for compositional analysis.

#### 2.10.7. Transmission electron microscopy (TEM)

All samples were fixed in the electron microscope station with conductive adhesive. Then, transmission electron microscopy (TEM) observations were carried out over a transmission electron microscope (Philips CM10 operating at 60 kV tension).

#### 2.10.8. UV-Vis measurements

UV-Vis absorption spectra were recorded on a Shimadzu UV-1800 model spectrophotometer.

#### 2.10.9. Dynamic light scattering (DLS)

The size distributions of the samples were determined by a Nano-ZS instrument (Malvern Instruments Ltd., UK).

### 3. Results and discussion

#### 3.1. Preparation and characterization of reactive monomers (Hal-V and MAH-β-CD) and Hal-V/MAH-β-CD hybrid nanocarrier

Cyclodextrin (β-CD)-functionalized halloysite nanotubes (Hal-V/MAH-β-CD) were prepared according to the steps outlined in Scheme 1. Firstly, Hal-V and MAH-β-CD as two important polymerizable monomers were prepared by reacting of Hal nanotubes and β-CD with 3-(trimethoxysilyl)propyl methacrylate and maleic anhydride, respectively. On the other hand, pristine Hal nanotubes were initially functionalized with silane coupling reagent via simple hydrolysis/condensation reaction. Then polymerizable β-CD derivative containing vinyl carboxylic acid functional groups were synthesized by a ring-opening reaction between β-CD and MAH. Finally, Hal-V/MAH-β-CD nanocarrier was obtained using free radical copolymerization in the presence of MBA as cross-linker. The successful synthesis of Hal-V, MAH-β-CD and Hal-V/MAH-β-CD nanocarrier were confirmed by using various physicochemical analyses.

From Fig S2B,  $^1H$  NMR spectrum of MAH-β-CD showed the characteristic peaks at 3.2–5.9 ppm corresponding to –CH–1, 2, 3, 4, 5, 6 and –OH groups of β-CD (Fig S2A) [41]. Moreover, the appearance of two new peaks at 6.30 and 6.46 ppm related to –CH=CH– group indicated the successful incorporation of MAH onto the β-CD backbone. In Fig S2C, the FTIR spectrum of MAH-β-CD was illustrated and compared with that of β-CD. The structure of β-CD can be clearly elucidated in the spectrum of the MAH-β-CD by ob-

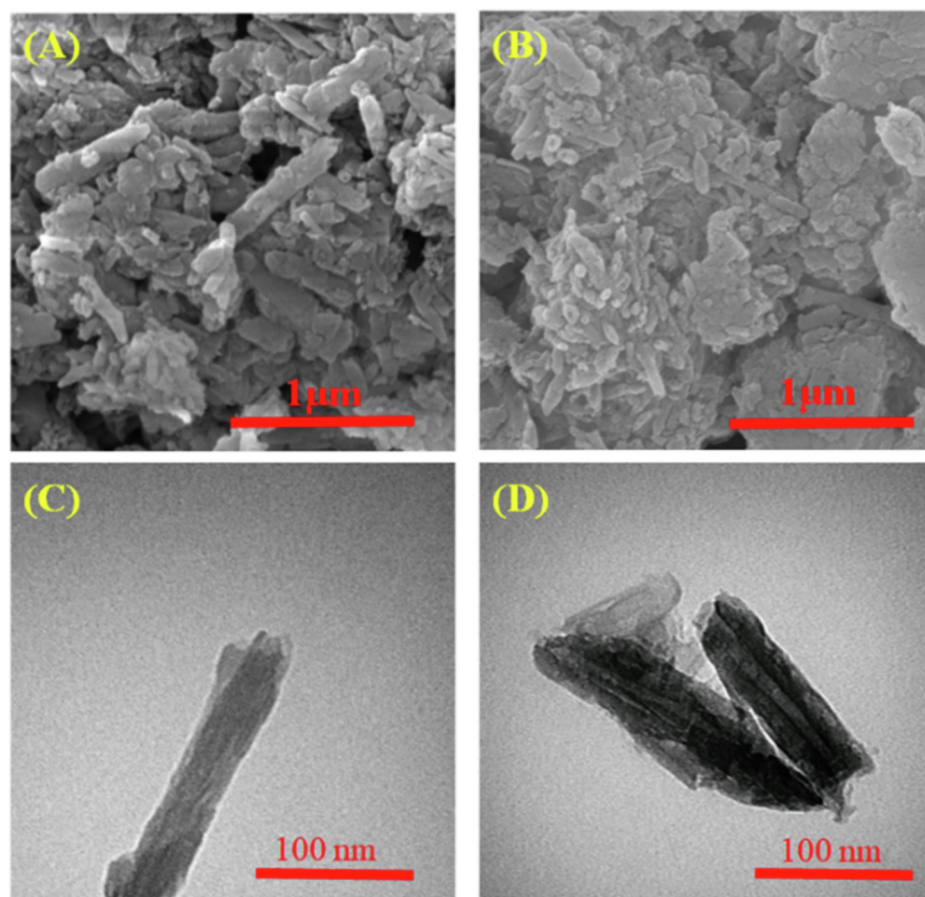
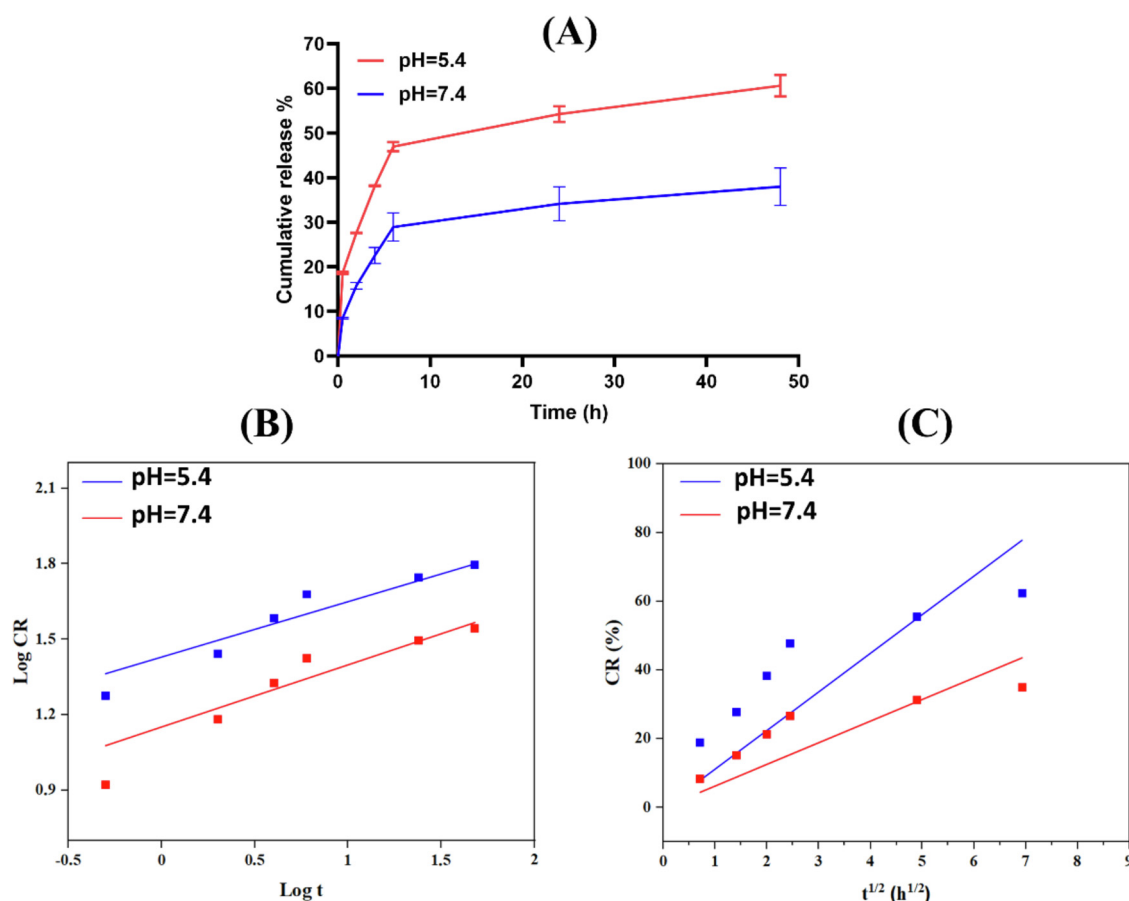


Fig. 2. The SEM images of (A) bare Hal, (B) Hal-V/MAH- $\beta$ -CD and the TEM images of (C) bare Hal, (D) Hal-V/MAH- $\beta$ -CD.

serving the peaks at  $1026\text{ cm}^{-1}$  and  $1150\text{ cm}^{-1}$ , that were indicative of glycosidic C–O–C stretching and coupled C–C/C–O stretching vibrations, respectively [42]. In the spectra of MAH- $\beta$ -CD, two new additional peaks at  $1628\text{ cm}^{-1}$  and  $1722\text{ cm}^{-1}$  were seen that could be assigned to the stretching vibration of C=C and C=O, respectively, indicating successful reaction of MAH with  $\beta$ -CD. In addition, the FTIR spectra of Hal-V/MAH- $\beta$ -CD and Hal-V were conducted and compared with bare Hal nanotube. From Fig 1A, all distinguished peaks related to Hal such as  $471\text{ cm}^{-1}$  (Al–O–Si deformation vibration),  $542\text{ cm}^{-1}$  (Si–O–Si deformation vibration),  $695\text{ cm}^{-1}$  and  $754\text{ cm}^{-1}$  (Si–O stretching vibration),  $912\text{ cm}^{-1}$  (O–H deformation vibration of inner Al–O–H groups),  $1034\text{ cm}^{-1}$  (Si–O–Si stretching vibration),  $1095\text{ cm}^{-1}$  (Si–O stretching vibration),  $1634\text{ cm}^{-1}$  and  $3443\text{ cm}^{-1}$  (O–H stretching vibration of adsorbed water) and  $3621\text{ cm}^{-1}$  and  $3695\text{ cm}^{-1}$  (O–H stretching vibrations of Al–OH groups) could be seen in the FTIR spectra of both Hal-V and Hal-V/MAH- $\beta$ -CD, suggesting that Hal structure was intact even after modification with silane group and incorporation of biopolymer [42]. However, the appearance of two new characteristic peaks at  $2895\text{ cm}^{-1}$  and  $1736\text{ cm}^{-1}$  in the Hal-V spectrum, corresponding to  $-\text{CH}_2$  and C=O functionalities, indicated its successful preparation [43]. After the polymerization, two new peaks at  $1565\text{ cm}^{-1}$  and  $1693\text{ cm}^{-1}$  were seen in the FTIR spectrum of Hal-V/MAH- $\beta$ -CD that could be assigned to N–H (bending) and C=O (stretching) vibrations of amide in the polymeric network [21]. To elucidate possible changes in the structure of Hal upon polymer decoration, the XRD pattern of nanocarrier was obtained and compared with that of bare Hal, Fig 1B. As depicted, the eight characteristic peaks at  $2\theta = 12.1^\circ$ ,  $20.1^\circ$ ,  $24.7^\circ$ ,  $26.5^\circ$ ,  $35.6^\circ$ ,  $38.4^\circ$ ,  $55.1^\circ$  and  $62.6^\circ$  corresponded to the structure of Hal (JCPDS No. 29–

1487) could be also detected in the XRD pattern of Hal-V/MAH- $\beta$ -CD by a decrease in the intensity [44]. Moreover, the XRD pattern of Hal-V/MAH- $\beta$ -CD showed no remarkable shift or change in the interlayer distance when compared with that of bare Hal, indicating the formation of crosslinked networks by growing the polymeric chains on the surface of Hal [43]. The effect of MAH- $\beta$ -CD polymerization on the surface properties of Hal was investigated using  $\text{N}_2$  adsorption-desorption isotherm of Hal-V/MAH- $\beta$ -CD (Fig 1C). Based on a previous report, the specific surface area and the pore diameter of bare Hal were found to be  $51\text{ m}^2\text{g}^{-1}$  and  $5.4\text{ nm}$ , respectively [43]. In this study, the specific surface area of Hal-V/MAH- $\beta$ -CD was  $48\text{ m}^2\text{g}^{-1}$ , indicating that functionalization of Hal surface by  $\beta$ -CD did not alter significantly the aforementioned value. In contrary, the pore diameter of nanocarrier was increased to  $12\text{ nm}$ . This could be explained that the resulted polymeric network provided higher porosity by the formation of inter-particle pores on the surface of Hal. The TGA analysis was exploited to study the thermal stability of bare Hal, Hal-V and Hal-V/MAH- $\beta$ -CD, as depicted in Fig 1D. Both bare Hal and Hal-V showed two main weight losses at around  $100^\circ\text{C}$  and  $550^\circ\text{C}$  corresponded to the loss of water and Hal structure dehydroxylation, respectively [45]. Compared to the thermogram of bare Hal, an observable weight loss ( $\sim 4\text{ wt.}\%$ , around at  $300^\circ\text{C}$ ) was occurred in the thermogram of Hal-V, which indicated the degradation of grafted silane. The weight loss of Hal-V/MAH- $\beta$ -CD was higher than those of Hal and Hal-V, which could be assigned to the successful coating of Hal surface with  $\beta$ -CD. Notably, the content of silane and  $\beta$ -CD were calculated to be  $4$  and  $12\text{ wt.}\%$ .

The SEM images of Hal and Hal-V/MAH- $\beta$ -CD were shown in Fig 2A and B, respectively, to investigate their direct surface visual-



**Fig. 3.** The cumulative release curve of the DOX@Hal-V/MAH- $\beta$ -CD at pH 7.4 and 5.4(A) and kinetic models for DOX release from nanocarrier: Korsmeyer-Peppas model (B) and Higuchi model (C).

izations. A neat tubular structure can be seen from Fig 2A for bare Hal. From Fig 2B, the comparison of the SEM images of Hal with Hal-V/MAH- $\beta$ -CD showed that upon introduction of  $\beta$ -CD on the surface of Hal, tubular shape did not change remarkably. However, it should be noticed that Hal-V/MAH- $\beta$ -CD exhibited more dense and compact morphology, which can be due to the intertwining of the polymeric chain. Furthermore, comparative TEM images from nanotubes before and after modifying  $\beta$ -CD were shown in Fig 2C and D, respectively. Observable clear changes could be seen from the TEM image of Hal-V/MAH- $\beta$ -CD. On the other hand, modifying  $\beta$ -CD not only, increased the thickness of the Hal nanotubes (about 10–15 nm), but also located on the surface of Hal as dark color layer in which caused the hollow tubular structure of Hal become less dateable. All these observations from SEM and TEM images are in good agreement with those reported results for Hal surface modification [46–48].

Furthermore, the results of DLS measurements to record the average hydrodynamic diameter of bare Hal and Hal-V/MAH- $\beta$ -CD were shown in Fig S3 A and B, respectively. The average hydrodynamic diameter of bare Hal was  $\sim$ 339.3 nm, while Hal-V/MAH- $\beta$ -CD possess an average diameter of 350.3 nm, which was 11.0 nm larger than bare Hal. The DLS size difference between bare Hal and Hal-V/MAH- $\beta$ -CD clearly demonstrated that the surface of Hal was coated with a thick  $\beta$ -CD layer.

### 3.2. DOX loading and release of Hal-v/MAH- $\beta$ -CD and kinetics modeling

In this study, DOX was loaded on Hal-V/MAH- $\beta$ -CD via physical adsorption for 24 h under stirring at neutral pH condition.

The loading efficiency of Hal-V/MAH- $\beta$ -CD is measured  $\sim$ 48.12% which is higher than that of pristine Hal ( $\sim$ 18.9%). It is obvious that the loading capacity of pristine Hal is limited [49], but the modification of Hal surface by  $\beta$ -CD could significantly increase the drug loading capacity. This fact is in a good agreement with a study that DOX loading capacity of Hal nanotubes was increased from 18.6% to 31.6% after coating with polyglycerol layer [12]. Basically, various parameters such as adsorption conditions, drug interactions, and the most importantly the structures and surface property of Hal nanotube have significant influence on the loading and release of DOX [13,50]. In vitro release profile of DOX from Hal-V/MAH- $\beta$ -CD was evaluated in PBS solutions at two different pH values (5.4 and 7.4), which simulated weak acidic tumor and neutral blood microenvironments, respectively [51]. As shown in Fig 3A, approximately, 36% of DOX was released after 8 h at pH 5.4, while only 24% of DOX was released at pH 7.4 as neutral condition during the same period. After that, the release rate of Hal-V/MAH- $\beta$ -CD reached a maximum value of 60% and 38% in 48 h at pH 5.4 and 7.4, respectively. It should be highlighted that the higher DOX release rate at low pH value (5.4) not only could be attributed to cavity change of Hal-V/MAH- $\beta$ -CD nanocarrier but also increased hydrophilicity of DOX (due to the protonation of its  $\text{NH}_2$  group), leading to fast release of DOX in acidic conditions. The same trend in DOX release behavior was observed in previous reports [12,14]. Therefore, the pH-dependent DOX release behavior of Hal-V/MAH- $\beta$ -CD nanocarrier can be clearly seen which is very important from chemotherapy point of view [52].

To clarify and understand the DOX release mechanism, the obtained in-vitro release data were analyzed using release kinetics

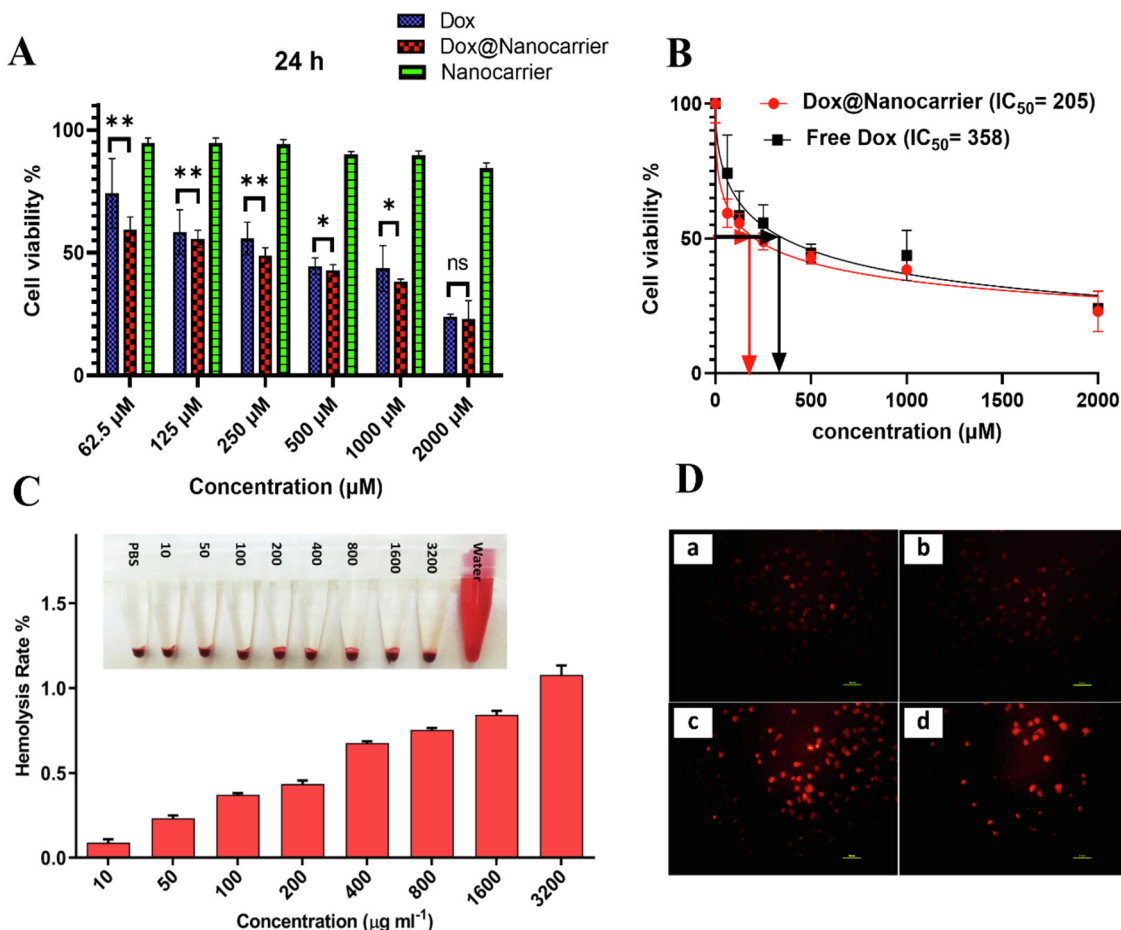


**Fig. 4.** Cytotoxicity of free DOX, DOX@nanocarrier and nanocarrier in-vitro on MCF-7 cells at different concentrations, \* $\rho < 0.05$ , \*\* $\rho < 0.01$ (A),The calculated IC<sub>50</sub> values using Graph Pad (prism) software (B). Hemocompatibility evaluation of nanocarrier (DI water and PBS as the positive and negative controls, respectively) and (C) fluorescent microscopy images for DOX@nanocarrier uptake by MCF-7 cells after 0.5 (a), 1 (b), 2 (c) and 3 h.

**Table 1**  
The calculated kinetic parameters of DOX release according to Higuchi and Korsmeyer-Peppas models.

Nanocarrier	Higuchi model	Korsmeyer-Peppas model				
		$K (h^{-1/2})$	$r^2$	$n$	$K (h^{-n})$	$r^2$
@Hal-V/MAH-β-CD	pH 5.4	11.24	0.17	0.22	26.9	0.93
	pH 7.4	6.297	0.35	0.25	14.2	0.92

models, namely Korsmeyer-Peppas (Eq. (1) and Fig 3B) and Higuchi (Eq. (2) and Fig 3C) [33,37].

$$Mt/M0 = K_{kp}t^n \tag{1}$$

$$F = K_H \times t^{1/2} \tag{2}$$

Based on Fig 3B and C, there is a better fit from Korsmeyer-Peppas equation, indicating that the release kinetics of DOX follow the Korsmeyer-Peppas model. Moreover, all parameters such as diffusion exponent (n), correlation coefficients (r<sup>2</sup>) and rate constants (k) were summarized in Table 1.

Since the n value is less than 0.45, it could be concluded that the DOX release mechanism is Fickian diffusion [53]. An obvious pH effect could be observed when comparing k values across the experiments. On the other hand, the k value in acidic environment was higher than that of pH 7.4, suggesting the higher release rate under acidic condition [54].

### 3.3. In-vitro cell cytotoxicity, blood compatibility and cell internalization of nanocarrier

Low cytotoxicity of drug nanocarriers in drug delivery systems is an essential key item, which is obtained from MTT assay results. Fig 4 A depicted the cytotoxic effect of free DOX, nanocarrier and DOX@nanocarrier on MCF-7 cells. As the results were exhibited, the synthesized nanocarrier (Hal-V/MAH-β-CD) has no remarkable cytotoxicity on MCF-7 cells, with greater than 95% cell viability even at a concentration of 2000 µM, suggesting the excellent non-toxicity and biologically friendly of Hal-V/MAH-β-CD nanocarrier. However, free DOX and DOX@nanocarrier illustrated cytotoxicity in a dose-dependent manner toward MCF-7 cells after 24 h incubation. Compared with free DOX, DOX@nanocarrier displayed higher toxicity as shown in Fig 4A. For instance, the cell viability of DOX@nanocarrier (250 µM) is 48% but free DOX is 62% at the same concentration. By increasing the concentration of DOX@nanocarrier, the cell viability decreased under 20% at the

concentration of 2000  $\mu\text{M}$ . Moreover, the half-maximal inhibitory concentration ( $\text{IC}_{50}$ ) values for free DOX and DOX@nanocarrier have been determined as 358  $\mu\text{M}$  and 205  $\mu\text{M}$ , respectively (Fig 4B). This can be attributed to the ability of nanocarrier to control the release of drug and gradual drug release inside the cells. These results showed that DOX loading in Hal-V/MAH- $\beta$ -CD nanocarrier facilitated its uptake in cancer cells, leading to higher toxicity when compared with free DOX. In addition to enhanced drug uptake, reduced drug efflux by multidrug resistance proteins could be another reason for higher drug accumulation when loaded in nanocarrier compared with free drug. Moreover, reduction in  $\text{IC}_{50}$  value and effective drug concentration can lead to inhibition of drug resistance development and damage to healthy tissues which is very crucial in chemotherapy.

Based on FDA recommendations, the biocompatibility evaluation of materials applied as drug carrier in intravenous injection is substantial and in-vitro hemolysis experiments should be conducted to test for hemolytic effect [55]. Previous reports showed an abnormal destruction of red blood cells (hemolysis) when RBCs were exposed to bare Hal nanotubes over a range of concentrations [56], and the fact could be easily decreased after surface modification of Hal by chitosan grafting and PEI grafting [16,57]. In this study, the dose-dependent hemolytic effects of Hal-V/MAH- $\beta$ -CD nanocarrier at the various concentrations ranging 10–3200  $\mu\text{g mL}^{-1}$  on RBCs were shown in Fig 4C. The hemolysis rate of Hal-V/MAH- $\beta$ -CD is less than 1.10% in all concentrations. This phenomenon indicated that Hal-V/MAH- $\beta$ -CD nanocarrier can be classified as non-hemolytic material according to national biological safety.

Due to fluorescent nature of DOX, DOX@Hal-V/MAH- $\beta$ -CD nanocarrier internalization can be easily observed by fluorescent microscopy to evaluate the qualitative cellular uptake into the MCF-7 cells. In this regard, nanocarrier-loaded with DOX (DOX@Hal-V/MAH- $\beta$ -CD) was exposed with MCF-7 cells in a time-dependent manner, as shown in Fig 4D, for 0.5, 1, 2 and 3 h. The images showed that the accumulation of DOX@Hal-V/MAH- $\beta$ -CD nanocarriers inside the cells was increased over the time, and could be considered as a clear witness for successful nanocarrier uptake by the cells.

#### 4. Conclusion

Taking the advantages of biocompatibility and easy functionalization of Hal nanotubes, for the first time, a novel pH-sensitive Hal-based nanocarrier (Hal-V/MAH- $\beta$ -CD), as a drug delivery system, was designed and prepared through simple free radical copolymerization of Hal-V and MAH- $\beta$ -CD in the presence of MBA for delivery of DOX to enhance the chemotherapeutic efficiency in MCF-7 breast cancer cells. Various characterization techniques were used to confirm the successful preparation of Hal-V/MAH- $\beta$ -CD hybrid nanomaterial. Hal-V/MAH- $\beta$ -CD nanocarrier showed higher DOX cumulative release in acidic medium (pH 5.4) than the neutral medium (pH 7.4). Based on cytotoxicity studies, DOX-loaded hybrid nanocarrier exhibited more cytotoxic effect than free DOX. Moreover, the cellular uptake studies by fluorescent microscopy validated successful cell internalization of DOX-loaded Hal-V/MAH- $\beta$ -CD. All aforementioned results in the current study implied that the surface modification of Hal nanotubes with  $\beta$ -CD not only increased its blood compatibility, but also could be effectively employed as a potent drug delivery system for cancer therapy.

#### Declaration of Competing Interest

The authors declare that they have no known competing financial interests or personal relationships that could have appeared to influence the work reported in this paper.

#### CRediT authorship contribution statement

**Vahid Shafiei-Irannejad:** Investigation, Writing – original draft. **Vahid Rahimkhoei:** Visualization, Investigation. **Morteza Molaparast:** Formal analysis. **Ali Akbari:** Conceptualization, Supervision, Writing – review & editing.

#### Acknowledgement

Authors would like to thank, Urmia University of Medical Sciences, Urmia, Iran for providing financial support. (Project number: 9851, approved by the Research Ethics Committee at the Urmia University of Medical Sciences, Ethical code: IR.UMSU.REC.1398.528).

#### Supplementary materials

Supplementary material associated with this article can be found, in the online version, at doi:10.1016/j.molstruc.2022.133004.

#### References

- [1] M. Al-Hajj, M.S. Wicha, A. Benito-Hernandez, S.J. Morrison, M.F. Clarke, Prospective identification of tumorigenic breast cancer cells, *Proc. Natl. Acad. Sci.* 100 (7) (2003) 3983–3988.
- [2] P. Chowdhury, P.K. Nagesh, E. Hatami, S. Wagh, N. Dan, M.K. Tripathi, S. Khan, B.B. Hafeez, B. Meibohm, S.C. Chauhan, Tannic acid-inspired paclitaxel nanoparticles for enhanced anticancer effects in breast cancer cells, *J. Colloid Interface Sci.* 535 (2019) 133–148.
- [3] K.M. Laginha, S. Verwoert, G.J. Charrois, T.M. Allen, Determination of doxorubicin levels in whole tumor and tumor nuclei in murine breast cancer tumors, *Clin. Cancer Res.* 11 (19) (2005) 6944–6949.
- [4] G. Minotti, P. Menna, E. Salvatorelli, G. Cairo, L. Gianni, Anthracyclines: molecular advances and pharmacologic developments in antitumor activity and cardiotoxicity, *Pharmacol. Rev.* 56 (2) (2004) 185–229.
- [5] D.D. Von Hoff, M.W. Layard, P. Basa, H.L. DAVIS Jr, A.L. Von Hoff, M. Rozenzweig, F.M. Muggia, Risk factors for doxorubicin-induced congestive heart failure, *Ann. Intern. Med.* 91 (5) (1979) 710–717.
- [6] E.A. Lefrak, J. Pit'ha, S. Rosenheim, J.A. Gottlieb, A clinicopathologic analysis of adriamycin cardiotoxicity, *Cancer* 32 (2) (1973) 302–314.
- [7] X. Yang, X. Zhang, Z. Liu, Y. Ma, Y. Huang, Y. Chen, High-efficiency loading and controlled release of doxorubicin hydrochloride on graphene oxide, *J. Phys. Chem. C* 112 (45) (2008) 17554–17558.
- [8] K. Butowska, A. Woziwodzka, A. Borowik, J. Piosik, Polymeric nanocarriers: a transformation in doxorubicin therapies, *Materials* 14 (9) (2021) 2135.
- [9] A. Shafei, W. El-Bakly, A. Sobhy, O. Wagdy, A. Reda, O. Aboelenin, A. Marzouk, K. El Habak, R. Mostafa, M.A. Ali, A review on the efficacy and toxicity of different doxorubicin nanoparticles for targeted therapy in metastatic breast cancer, *Biomed. Pharmacother.* 95 (2017) 1209–1218.
- [10] J. Rezaie, A. Akbari, V. Rahimkhoei, Z.M. Lighvani, H. Jafari, Halloysite nanotubes/carbohydrate-based hydrogels for biomedical applications: from drug delivery to tissue engineering, *Polym. Bull.* (2021).
- [11] K. Fakhrudin, R. Hassan, M.U.A. Khan, S.N. Allisha, S.I. Abd Razak, M.H. Zreagat, H.F.M. Latip, M.N. Jamaludin, A. Hassan, Halloysite nanotubes and halloysite-based composites for biomedical applications, *Arabian J. Chem.* 14 (9) (2021) 103294.
- [12] X. Mo, F. Wu, B. Yu, W. Wang, X. Cai, Folate-PG modified halloysite nanotube for enhancing tumor targeting and anticancer efficacy, *Appl. Clay Sci.* 193 (2020) 105664.
- [13] J. Yang, Y. Wu, Y. Shen, C. Zhou, Y.-F. Li, R.-R. He, M. Liu, Enhanced therapeutic efficacy of doxorubicin for breast cancer using chitosan oligosaccharide-modified halloysite nanotubes, *ACS Appl. Mater. Interfaces* 8 (40) (2016) 26578–26590.
- [14] Y.-P. Wu, J. Yang, H.-Y. Gao, Y. Shen, L. Jiang, C. Zhou, Y.-F. Li, R.-R. He, M. Liu, Folate-conjugated halloysite nanotubes, an efficient drug carrier, deliver doxorubicin for targeted therapy of breast cancer, *ACS Appl. Nano Mater.* 1 (2) (2018) 595–608.
- [15] Z. Long, Y.-P. Wu, H.-Y. Gao, Y.-F. Li, R.-R. He, M. Liu, Functionalization of halloysite nanotubes via grafting of dendrimer for efficient intracellular delivery of siRNA, *Bioconjug. Chem.* 29 (8) (2018) 2606–2618.
- [16] Z. Long, J. Zhang, Y. Shen, C. Zhou, M. Liu, Polyethyleneimine grafted short halloysite nanotubes for gene delivery, *Mater. Sci. Eng.: C* 81 (2017) 224–235.
- [17] J. Rezaie, A. Akbari, Functionalization of halloysite nanotubes via grafting of polyhedral oligomeric silsesquioxane (POSS) nanoparticles for paclitaxel drug delivery, *Mater. Lett.* 315 (2022) 131942.
- [18] S. Manivannan, R. Ramaraj, Synthesis of cyclodextrin-silicate sol-gel composite embedded gold nanoparticles and its electrocatalytic application, *Chem. Eng. J.* 210 (2012) 195–202.
- [19] H.L. Ramirez, A. Valdivia, R. Cao, J.J. Torres-Labandeira, A. Fragoso, R. Villalonga, Cyclodextrin-grafted polysaccharides as supramolecular carrier systems for naproxen, *Bioorg. Med. Chem. Lett.* 16 (6) (2006) 1499–1501.

- [20] A.Z.M. Badruddoza, M.T. Rahman, S. Ghosh, M.Z. Hossain, J. Shi, K. Hidajat, M.S. Uddin,  $\beta$ -Cyclodextrin conjugated magnetic, fluorescent silica core-shell nanoparticles for biomedical applications, *Carbohydr. Polym.* 95 (1) (2013) 449–457.
- [21] X. Li, J. Chen, H. Liu, Z. Deng, J. Li, T. Ren, L. Huang, W. Chen, Y. Yang, S. Zhong,  $\beta$ -Cyclodextrin coated and folic acid conjugated magnetic halloysite nanotubes for targeting and isolating of cancer cells, *Colloids Surf. B* 181 (2019) 379–388.
- [22] N. Sabbagh, A. Akbari, N. Arsalani, B. Eftekhari-Sis, H. Hamishekar, Halloysite-based hybrid bionanocomposite hydrogels as potential drug delivery systems, *Appl. Clay Sci.* 148 (2017) 48–55.
- [23] Z. Bahrami, A. Akbari, B. Eftekhari-Sis, Double network hydrogel of sodium alginate/polyacrylamide cross-linked with POSS: swelling, dye removal and mechanical properties, *Int. J. Biol. Macromol.* 129 (2019) 187–197.
- [24] B. Eftekhari-Sis, V. Rahimkhoei, A. Akbari, H.Y. Araghi, Cubic polyhedral oligomeric silsesquioxane nano-cross-linked hybrid hydrogels: synthesis, characterization, swelling and dye adsorption properties, *React. Funct. Polym.* 128 (2018) 47–57.
- [25] F. Kazeminava, N. Arsalani, A. Akbari, POSS nanocrosslinked poly (ethylene glycol) hydrogel as hybrid material support for silver nanocatalyst, *Appl. Organomet. Chem.* 32 (6) (2018) e4359.
- [26] A. Akbari, N. Arsalani, Organic-Inorganic Incompletely Condensed Polyhedral Oligomeric Silsesquioxane-Based Nanohybrid: synthesis, Characterization and Dye Removal Properties, *Polym. Plast. Technol. Eng.* 55 (15) (2016) 1586–1594.
- [27] A. Akbari, N. Arsalani, Preparation and characterization of novel hybrid nanocomposites by free radical copolymerization of vinyl pyrrolidone with incompletely condensed polyhedral oligomeric silsesquioxane, *J. Inorg. Organomet. Polym. Mater.* 26 (3) (2016) 536–544.
- [28] B. Eftekhari-Sis, A. Akbari, P.Y. Motlagh, Z. Bahrami, N. Arsalani, Dye adsorption on cubic polyhedral oligomeric silsesquioxane-based poly(acrylamide-co-itaconic acid) hybrid nanocomposites: kinetic, thermodynamic and isotherms studies, *J. Inorg. Organomet. Polym. Mater.* 28 (5) (2018) 1728–1738.
- [29] N. Arsalani, A. Akbari, M. Amini, E. Jabbari, S. Gautam, K.H. Chae, POSS-based covalent networks: supporting and stabilizing Pd for Heck reaction in aqueous media, *Catal Lett.* 147 (4) (2017) 1086–1094.
- [30] M. Soleymani, A. Akbari, G.R. Mahdavinia, Magnetic PVA/laponite RD hydrogel nanocomposites for adsorption of model protein BSA, *Polym. Bull.* 76 (5) (2019) 2321–2340.
- [31] N. Arsalani, F. Kazeminava, A. Akbari, H. Hamishekar, E. Jabbari, H.S. Kafil, Synthesis of polyhedral oligomeric silsesquioxane nano-crosslinked poly(ethylene glycol)-based hybrid hydrogels for drug delivery and antibacterial activity, *Polym. Int.* 68 (4) (2019) 667–674.
- [32] A. Akbari, A. Naderahmadian, B. Eftekhari-Sis, Silver and copper nanoparticles stabilized on ionic liquids-functionalized polyhedral oligomeric silsesquioxane (POSS): highly active and recyclable hybrid catalysts, *Polyhedron* 171 (2019) 228–236.
- [33] S. Alinavaz, G.R. Mahdavinia, H. Jafari, M. Hazrati, A. Akbari, Hydroxyapatite (HA)-based hybrid bionanocomposite hydrogels: ciprofloxacin delivery, release kinetics and antibacterial activity, *J. Mol. Struct.* 1225 (2021) 129095.
- [34] A. Akbari, M. Padervand, E. Jalilian, F. Seidi, Sodium alginate-halloysite nanotube gel beads as potential delivery system for sunitinib malate anticancer compound, *Mater. Lett.* 274 (2020) 128038.
- [35] H. Jafari, M. Hassanpour, A. Akbari, J. Rezaie, G. Gohari, G.Reza Mahdavinia, E. Jabbari, Characterization of pH-sensitive chitosan/hydroxypropyl methylcellulose composite nanoparticles for delivery of melatonin in cancer therapy, *Mater. Lett.* 282 (2021) 128818.
- [36] V. Rahimkhoei, A. Akbari, M. Zirak, B. Eftekhari-Sis, Ag nanoparticles stabilized on cubic polyhedral oligomeric silsesquioxane cross-linked poly(N-isopropyl acrylamide-co-itaconic acid): an efficient catalyst for 4-nitrophenol reduction, *Funct. Mater. Lett.* 13 (07) (2020) 2051040.
- [37] M. Hassanpour, H. Jafari, S. Sharifi, J. Rezaie, Z.M. Lighvan, G.R. Mahdavinia, G. Gohari, A. Akbari, Salicylic acid-loaded chitosan nanoparticles (SA/CTS NPs) for breast cancer targeting: synthesis, characterization and controlled release kinetics, *J. Mol. Struct.* 1245 (2021) 131040.
- [38] A. Akbari, H. Jafari, G. Gohari, G. Kheiri, G.R. Mahdavinia, Fulvic acid-embedded poly (vinyl alcohol)-zinc oxide hydrogel nanocomposite: synthesis, characterization, swelling and release kinetic, *Int. Nano Lett.* (2021).
- [39] C. Su, H. Li, Y. Shi, G. Wang, L. Liu, L. Zhao, R. Su, Carboxymethyl- $\beta$ -cyclodextrin conjugated nanoparticles facilitate therapy for folate receptor-positive tumor with the mediation of folic acid, *Int. J. Pharm.* 474 (1–2) (2014) 202–211.
- [40] M. Rahimi, V. Shafiei-Irannejad, K.D. Safa, R. Salehi, Multi-branched ionic liquid-chitosan as a smart and biocompatible nano-vehicle for combination chemotherapy with stealth and targeted properties, *Carbohydr. Polym.* 196 (2018) 299–312.
- [41] H. Zhao, J. Gao, R. Liu, S. Zhao, Stimulus-responsiveness and methyl violet release behaviors of poly(NIPAAm-co-AA) hydrogels chemically crosslinked with  $\beta$ -cyclodextrin polymer bearing methacrylates, *Carbohydr. Res.* 428 (2016) 79–86.
- [42] S. Yang, P. Zong, J. Hu, G. Sheng, Q. Wang, X. Wang, Fabrication of  $\beta$ -cyclodextrin conjugated magnetic HNT/iron oxide composite for high-efficient decontamination of U (VI), *Chem. Eng. J.* 214 (2013) 376–385.
- [43] S. Sadjadi, M. Atai, Palladated halloysite hybridized with photo-polymerized hydrogel in the presence of cyclodextrin: an efficient catalytic system benefiting from nanoreactor concept, *Appl. Organomet. Chem.* 33 (3) (2019) e4776.
- [44] P. Yuan, P.D. Southon, Z. Liu, M.E. Green, J.M. Hook, S.J. Antill, C.J. Kepert, Functionalization of halloysite clay nanotubes by grafting with  $\gamma$ -aminopropyltriethoxysilane, *J. Phys. Chem. C* 112 (40) (2008) 15742–15751.
- [45] S. Bordeepong, D. Bhongsuwan, T. Punggrassami, T. Bhongsuwan, Characterization of halloysite from Thung Yai District, Nakhon Si Thammarat Province, in Southern Thailand, *Songklanakarin J. Sci. Technol.* 33 (5) (2011).
- [46] H. Wei, H. Wang, H. Chu, J. Li, Preparation and characterization of slow-release and water-retention fertilizer based on starch and halloysite, *Int. J. Biol. Macromol.* 133 (2019) 1210–1218.
- [47] S. Sadjadi, M. Atai, Ternary hybrid system of halloysite nanotubes, polyacrylamides and cyclodextrin: an efficient support for immobilization of Pd nanoparticles for catalyzing coupling reaction, *Appl. Clay Sci.* 153 (2018) 78–89.
- [48] H. Li, X. Zhu, J. Xu, W. Peng, S. Zhong, Y. Wang, The combination of adsorption by functionalized halloysite nanotubes and encapsulation by polyelectrolyte coatings for sustained drug delivery, *RSC Adv.* 6 (59) (2016) 54463–54470.
- [49] M. Liu, Z. Jia, D. Jia, C. Zhou, Recent advance in research on halloysite nanotubes-polymer nanocomposite, *Prog. Polym. Sci.* 39 (8) (2014) 1498–1525.
- [50] L. Li, H. Fan, L. Wang, Z. Jin, Does halloysite behave like an inert carrier for doxorubicin? *RSC Adv.* 6 (59) (2016) 54193–54201.
- [51] N. Raghunand, X. He, R. Van Sluis, B. Mahoney, B. Baggett, C. Taylor, G. Paine-Murrieta, D. Roe, Z. Bhujwalla, R. Gillies, Enhancement of chemotherapy by manipulation of tumour pH, *Br. J. Cancer* 80 (7) (1999) 1005–1011.
- [52] W. Fan, Y. Xu, Z. Li, Q. Li, Folic acid-modified  $\beta$ -cyclodextrin nanoparticles as drug delivery to load DOX for liver cancer therapeutics, *Soft. Mater.* 17 (4) (2019) 437–447.
- [53] P. Dramou, M. Fizir, A. Taleb, A. Itatahine, N.S. Dahiru, Y.A. Mehdi, L. Wei, J. Zhang, H. He, Folic acid-conjugated chitosan oligosaccharide-magnetic halloysite nanotubes as a delivery system for camptothecin, *Carbohydr. Polym.* 197 (2018) 117–127.
- [54] Q. Chen, J. Zheng, X. Yuan, J. Wang, L. Zhang, Folic acid grafted and tertiary amino based pH-responsive pentablock polymeric micelles for targeting anti-cancer drug delivery, *Mater. Sci. Eng.: C* 82 (2018) 1–9.
- [55] M. Rahimi, R. Karimian, E. Mostafidi, E.B. Noruzi, S. Taghizadeh, B. Shokouhi, H.S. Kafil, Highly branched amine-functionalized p-sulfonatocalix [4]arene decorated with human plasma proteins as a smart, targeted, and stealthy nano-vehicle for the combination chemotherapy of MCF7 cells, *New J. Chem.* 42 (15) (2018) 13010–13024.
- [56] H.-Y. Liu, L. Du, Y.-T. Zhao, W.-Q. Tian, *In vitro* hemocompatibility and cytotoxicity evaluation of halloysite nanotubes for biomedical application, (2015).
- [57] M. Liu, Y. Chang, J. Yang, Y. You, R. He, T. Chen, C. Zhou, Functionalized halloysite nanotube by chitosan grafting for drug delivery of curcumin to achieve enhanced anticancer efficacy, *J. Mater. Chem. B* 4 (13) (2016) 2253–2263.